JJMIE

Volume 11 Number 4, December. 2017
ISSN 1995-6665
Pages 235 -243

Jordan Journal of Mechanical and Industrial Engineering

Modeling and Simulation of Shrouded Horizontal Axis Wind Turbine Using RANS Method

C. Ghenai [a *], T. Salameh [b], I. Janajreh [b]

[a] *Sustainable and Renewable Energy Engineering Department, College of Engineering- University of Sharjah, Sharjah 27272, United Arab Emirates*

[b] *Mecanical Engineering Program, Khalifa University of Science and Technology, Masdar Institute- Abu Dhabi, 54224, United Arab Emirates*

Abstract

The vast deployment of wind energy leads to its technical maturity and cost reduction that compete with natural gas. Low wind regions can be also targeted when shrouded or optimally designed turbine is utilized. The objective of the present study is to assess the performance of the shrouded Horizontal Axis Wind Turbine (HAWT) numerically subjected to low wind speed. The goal is to develop wind energy technologies that can maximize the power extracted from the turbine under low wind conditions. Three blades horizontal axis wind turbine surrounded with a shroud was tested in the present study. The Reynolds Averaged Navies-Stokes (RANS) modeling approach and finite volume numerical method was used to solve the governing equations. These equations are based on the equations of conservation of mass, momentum and turbulence scalars (k-□). The flow field around the wind turbine and inside the shroud was resolved. The induction factor was obtained from the computed velocity profiles. The turbine power coefficient (Cp) was determined using the induction factor. A comparison between the Cp with and without shroud at different tip speed ratios is presented in the present paper. The results show that the shrouded turbines can generate quadruple of the power of the non-shrouded baseline HAWT.

1. Introduction

Nearly eighty two percent of the world energy demand (electricity generation, transportation, buildings, and industrial applications) is provided through the non-renewable and unsustainable fossil fuels, i.e., coal, oil and natural gas. Renewable and clean energy systems continue to evolve and deploy to mitigate the problems of climate change (high GHS emissions from combustion of fossil fuels), energy security, the raising future energy demand, and the depletion of fossil fuel resources (oil, natural gas and coal) [1]. A comparison between the resource intensities (material, area, energy, CO_2 and capital intensities related to the construction of renewable energy systems) and operational parameters (system efficiency, capacity factor, and lifetime) of fossil fuel, renewable and nuclear power systems has been presented by Ghenai and Janajreh [1]. Among these renewable energy technologies, wind energy will continue to play an important role in the future. According to the World Wind Energy Association, the world has seen a new record (63.69 GW) in its installations in 2015 and nearly covering 3% of the global electricity supply in 2012 [2]. It also observed global growth rate of 17.2 % in 2015. The world total wind capacity reached 435 GW in 2015, with 46.2%, 33%, 29%, and 25.45 increases in Brazil, Poland, China, and Turkey, respectively (most dynamic countries with the strongest growth rates in 2015). This growth can be accelerated in the future should renewable energy policies continue to emerge from countries around the world [3].

While wind intermittency and low speed reduce turbine capacity factor, shrouded wind turbine can mitigate this loss and help in increasing wind energy deployment. This technology can be adopted to generate higher power in regions characterized with low speed conditions. The turbine is enclosed in shroud or duct that will allow the turbine to operate at higher efficiencies and thereby capacity compared to non-shrouded turbine. The shroud is used to increase the flow velocity or the volume of airflow around the turbine. More power is then generated with greater return in investment.

Hjort and Larsen [4] investigated the design requirement for Diffuser Augmented Wind Turbine (DAWT) rotor to efficiently convert the available energy shaft energy. Three different configurations were studied: bare propeller (HAWT), classical diffuser augmenter wind turbine (DAWT) and high performance multi element DAWT. The results showed that the DAWT rotors can successfully convert the available energy to shaft energy if the swirl and axial loading distribution were selected correctly.

Bala [5] performed experimental and numerical study of diffuser augmented wind turbine. The wind turbine power performance was evaluated using the power coefficient values. The experimental date showed

* Corresponding author e-mail: cghenai@sharjah.ac.ae.

improvements for the electrical power values, resulting in an average of 90% in the power coefficient and the more pronounced enhancement was obtained at low wind speed values [5].

A shrouded wind turbine generating high output power with wind lens technology was investigated by Yuji Ohya and Takahi Karasudani [6]. They showed that the shrouded wind turbine with brimmed diffuser augmented the power by 2-5 compared to bare wind turbine for given wind speed and rotor diameter. This is due to low-pressure region, due to the strong vortex formation behind the broad brim leading to draw more mass flow to the wind turbine inside the diffuser shroud.

Kosasih and Tondelli [7] focused, in their study, on the effects of diffuser shape and geometries, and blade airfoils on the wind turbine performance enhancement. Three different geometrical features: straight diffuser, nozzle-diffuser combination, and brimmed diffuser combination have been investigated. The tests confirmed that placing the micro turbine model inside a shroud can substantially improve its performance. The results showed that the diffuser shroud improves the performance by 60% compared to the bare turbine. The nozzle-diffuser enhancement was 63% slightly better than diffuser only. The findings from their work suggested that shrouding micro wind turbine not only improves its performance, but also provide guidelines on the design of the diffuser geometrical parameters (L/D) and/or (H/D) with a customized performance curve.

Hu and Wang [8] used a self-adaptive flange for the wind turbine shroud. The self-adaptive flange can maintain the advantages of the flanged diffuser at wind velocities lower than the rated velocity and reduce the wind loads acting on the diffuser and blades at higher wind velocities. Numerical results show that the wind load acting on the total flanged diffuser can be reduced by about 35% at 60 m/s due to the reconfiguration of the self-adaptive flange.

Aniket *et al.* [9] investigated the flow and performance of shrouded turbines using Reynolds Averaged Navier-Stokes (RANS) equations. Different shroud geometries were evaluated for their augmentation of mass flow through the turbine. The results showed an augmentation ratios of up to 1.9 can be achieved with shrouded turbines.

El-Zahaby *et al.* [9-10] used 2D axisymmetric CFD model of flanged diffuser as a casing for small wind turbines to increase the generated power. The numerical simulation shows the creation of vortices behind flange that cause pressure drop which increases mass flow rate through the diffuser leading to an increase in the generated power.

The main objective of the present study is to perform numerical simulations to test the performance of shrouded horizontal axis wind turbine under the low speed wind conditions of the Arabian Peninsula eastern coastline as indicated elsewhere with an average annual wind at the borderline cut-in wind turbine speed of 4.5 m/s [11]. The goal is to develop wind energy technologies that can maximize the power extracted from the turbine under low wind conditions and to accelerate the penetration of wind energy technologies in the Arabian Peninsula.

2. Governing Equations

A steady state solution is sought for the rotating turbine. This can be achieved through a "rotating reference frame" formulation in which the turbine rotor rotation is assigned a specific rotating speed without need to temporally trace its time advancement. This can drastically reduce the computational time and remove the burden in carrying sensitivity studies. Although the details of the flow due to the rotating blade against the outer domain and there interaction in generated vorticity trails will be undermined, nevertheless an average of these phenomena is captured at lower cost than the lengthy real time transient calculation. These latter real time calculations follow transient arbitrary Lagrangian Formulation, which involves domain movement and mesh sliding as appears in a previous work by the present authors [12], are limited to smaller flow domain to bring more flow insight or its physics validation. The equations of conservation of mass, momentum, and the two scale turbulence equations (turbulent kinetic energy k and the dissipation of the kinetic energy ε) are solved to predict the flow field around the wind turbine [13-14]. The time averaged gas phase equations for steady turbulent flow are:

$$\frac{\partial}{\partial x_j}\left(\rho u_i \Phi\right) = -\frac{\partial}{\partial x_i}\left(\Gamma_\Phi \frac{\partial \phi}{\partial x_i}\right) + S_\Phi \tag{1}$$

where Φ is the dependent variable that can represent the velocity u_i, the turbulent kinetic energy k, and the dissipation rate of the turbulent kinetic energy ε. The governing equations in steady state form are given such that, the conservation of energy is written as:

$$\frac{\partial \overline{\rho\, u_i}}{\partial x_i} = 0 \tag{2}$$

where ρ is the density, u_i are the three velocity components. The momentum equation is written as:

$$\frac{\partial\left(\overline{\rho u_i u_j}\right)}{\partial x_j} = -\frac{\partial \overline{P}}{\partial x_i} + \frac{\partial\left(\overline{t_{ij}} + \overline{\tau_{ij}}\right)}{\partial x_j} \tag{3}$$

where is the p is the static pressure and $\bar{t}_{ij}$ is the viscous stress tensor defined as:

$$\bar{t}_{ij} = \mu\left[\left(\frac{\partial \overline{u_i}}{\partial x_j} + \frac{\partial \overline{u_j}}{\partial x_i}\right) - \frac{2}{3}\frac{\partial \overline{u_k}}{\partial x_k}\delta_{ij}\right]$$

$\delta_{ij} = 1 \text{ if } i = j \text{ and } \delta_{ij} = 0 \text{ if } i \neq j$

$\bar{\tau}_{ij}$ is the average Reynolds stress tensor defined and modeled using the eddy viscosity turbulence model as:

$$\bar{\tau}_{ij} = -\overline{\rho\, u_i' u_j'}$$

$$\overline{\tau_{ij}} = \mu_t\left[\left(\frac{\partial \overline{u_i}}{\partial x_j} + \frac{\partial \overline{u_j}}{\partial x_i}\right) - \frac{2}{3}\frac{\partial \overline{u_k}}{\partial x_k}\delta_{ij}\right] - \frac{2}{3}\left(\overline{\rho\, k\, \delta_{ij}}\right)$$

where k is the average turbulent kinetic energy defined as:

$$\bar{k} = \frac{1}{2}\overline{u_i' u_i'}$$

and μ_t is the turbulent eddy viscosity expressed in terms of k and the dissipation rate (ε) as:

$$\mu_t = c_\mu \frac{\overline{\rho k^2}}{\overline{\varepsilon}}$$

where C_μ is constant (C_μ = 0.09) and $\overline{\varepsilon}$ is the average dissipation rate of the turbulent kinetic energy and defined as:

$$\overline{\varepsilon} = \nu \overline{\frac{\partial u_i'}{\partial x_j} \frac{\partial u_i'}{\partial x_j}}$$

where ν is the kinematic viscosity. The two scalar transport equations for each of the Turbulence Kinetic Energy (k) and its dissipation are written as (ε):

$$\frac{\partial\left(\overline{\rho k u_i}\right)}{\partial x_i} = \frac{\partial\left[\left(\mu + \frac{\mu_t}{\sigma_k}\right)\frac{\partial \overline{k}}{\partial x_j}\right]}{\partial x_j} + G_k - \overline{\rho \varepsilon} \tag{4}$$

where σ_k = 1 and G_k is the production of the turbulent kinetic energy defined as:

$$G_k = \mu_t\left[\left(\frac{\partial \overline{u_i}}{\partial x_j} + \frac{\partial \overline{u_j}}{\partial x_i}\right)\right]\frac{\partial \overline{u_i}}{\partial x_j} - \frac{2}{3}\frac{\partial \overline{u_i}}{\partial x_j}\delta_{ij}\left[\mu_t \frac{\partial \overline{u_k}}{\partial x_k} + \overline{\rho k}\right]$$

$$\frac{\partial\left(\overline{\rho\, \varepsilon\, u_j}\right)}{\partial x_i} = C_{\varepsilon 1}\frac{\overline{\varepsilon}}{k}G_k + \frac{\partial\left[\left(\mu + \mu_t/\sigma_\varepsilon\right)\left(\partial\overline{\varepsilon}/\partial x_j\right)\right]}{\partial x_j} - C_{\varepsilon 2}\,\overline{\rho}\frac{\overline{\varepsilon}^2}{k} \tag{5}$$

where $C_{\varepsilon 1}$=1.44, $C_{\varepsilon 2}$ =1.92, and σ_ε=1.3 are the tuning model constants.

3. Geometry, Bounadar Conditions, Mesh and Numerical Method

Fig. 1 shows a schematic of the three dimensional wind turbine. The wind turbine blade characteristics are summarized in Table 1. For the boundary conditions, the air enters from the left boundary at a velocity U_{wu} (Inlet flow – velocity inlet). The computational domain has a cylindrical shape as shown in Fig. 1 (symmetry). The air exits the computational domain from the right side (Outflow). The rotor is modeled as rotating immersed frame with and angular velocity ω [rad/s] which remove the hassle of seeking transient analyses. Thus, an averaged steady state solution is sought. The geometry of the shroud is shown in Fig. 2. The shroud characteristics are summarized in Table 1.

A Quality mesh was generated for the shrouded and unshrouded turbines. The number of nodes selected for the wind turbine simulation study was 188,000. A grid independent study was performed with three different meshes (coarse mesh with 94,000 nodes, medium mesh with 188,000 nodes and fine mesh with 365,000 nodes) and the results of the simulation were compared. The difference between the simulations results obtained with medium and fine mesh was less than 1.5%. Based on this grid independent study, the medium mesh was selected for this numerical study. A control volume based finite difference method is used in order to solve a system of partial differential equations governing the conservation of mass, momentum, and turbulent flow. In this CFD analysis, the SIMPLER algorithm is used to solve explicitly for the velocity and pressure fields. SIMPLER (revised version of SIMPLE algorithm) is a semi-implicit method used as a numerical procedure for solving the Navier-Stokes equations [15-17]. The SIMPLE algorithm uses a relationship between velocity and pressure corrections (pressure-velocity coupling algorithm) to enforce the continuity equation (mass conservation) and to obtain the pressure field.

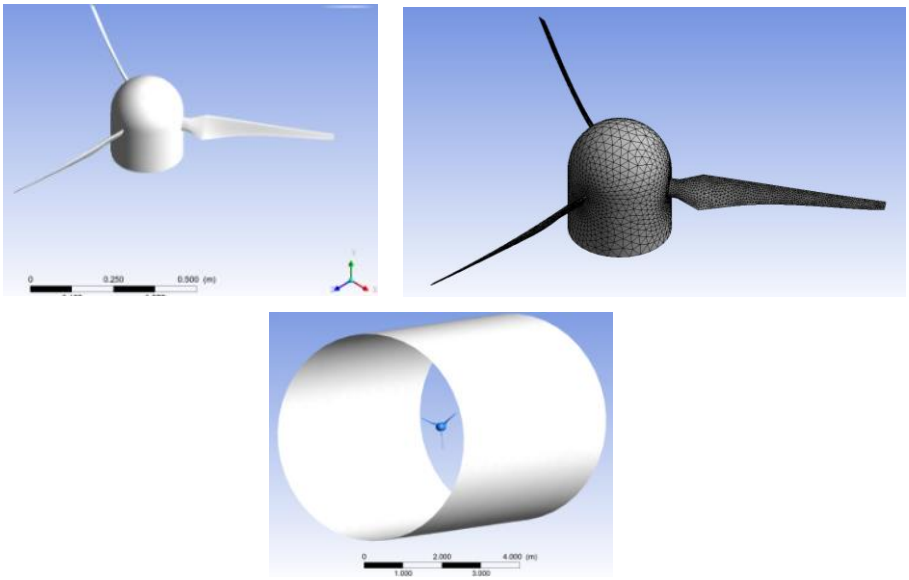

Figure 1: Unshrouded wind turbine geometry, mesh and computational domain

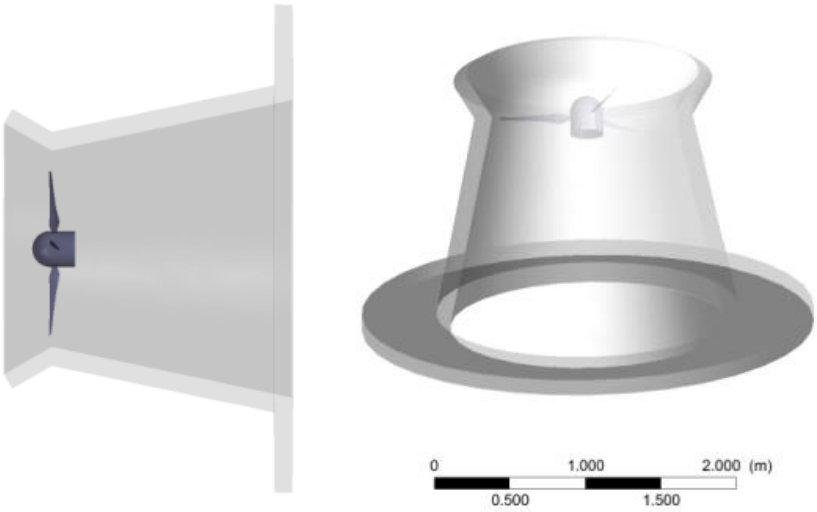

Figure 2: Shrouded Wind Turbine Geometry

Table 1: Wind turbine and shroud characteristics

Blade - airfoil	SG6043
Blade length (m)	0.5
Throat diameter D (m)	1.17
Rotor diameter	1.16
Diffuser Length L (m)	1.46
Diffuser angle	12°

4. Performance Characteristics of the Wind Turbine

4.1. Unshrouded Baseline Wind Turbine

The efficiency of the wind turbine represented by the power coefficient, C_p, and the power extracted from the turbine, P_t, are used as the performance characteristics of the wind turbine. The power coefficient is given by:

$$C_p = \frac{P_t}{P_{wind}} = \frac{T.\omega}{P_{wind}} \quad (6)$$

where T is the torque (N.M), ω is the angular velocity of the turbine (rad/s), and P_{wind} is the maximum available power in the wind (W). The wind power is given by:

$$P_{wind} = 0.5\,\rho\,A\,U_w^3 \quad (7)$$

where ρ is the air density (kg/m^3), A is the rotor diameter (m^2) and U_w is the wind speed.

The C_p is also given [12] by:

$$C_p = 4\,a\,(1-a)^2 \quad (8)$$

where the induction factor *a* is given by:

$$a = 1 - \frac{U_{wrot}}{U_{wu}} \quad (9)$$

$$U_{wrot} = \frac{1}{2}(U_{wu} + U_{wd}) \quad (10)$$

where $U_{wrot}, U_{wu}, and\ U_{wd}$ are the air velocities at the rotor, up-steam and down-stream of the turbine blades, respectively.

4.2. Shrouded Wind Turbine

The power coefficient of the shrouded wind turbine [6, 18, 19] is given by:

$$C_p = \epsilon_L\ \mu\, 4\,\bar{a}\,(1-\bar{a})^2 \quad (11)$$

$$\epsilon_L = \frac{A_{out}}{A_{rot}} \quad (12)$$

$$\mu = \frac{U_{out}}{U_{wu}} \quad (13)$$

$$\bar{a} = 1 - \frac{U_{wd}}{U_{wu}} \quad (14)$$

$$C_{p)Diffuser} = \mu\, 4\,\bar{a}\,(1-\bar{a})^2 \quad (15)$$

where A_{out} and A_{rot} are the surface areas at the exit from the shroud and at the rotor (see Fig. 3), ε_L and μ are the area ratio and the back pressure coefficient, and $Cp)_{Diffuser}$ is the power coefficient due to the diffuser.

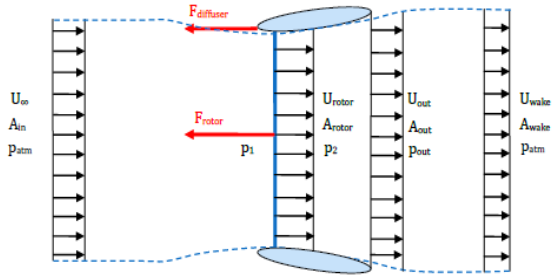

Figure 3: Control volume for shrouded turbine [17-18]

5. Results

The simualtion results of the unshrouded and shrouded turbine are evaluated and presneted. The effect of turbine tip speed ratio (TSR = 4 – 10) on the power extracted and the Cp is investigated in the present study. The wind speed at the inlet of the computaional domain was set to as low as U_{wu} = 4 m/s and the corrosponding rotational speed ω (rad/s) of the turbine was determined from the tip speed ratio equation (TSR = ω.R/U_{wu}, where R is the blade length). Fig. 4 shows the velocity magnitude of the air flow at the positon of the unshrouded wind turbine (y =0) and behinde the wind turbine (y = 0.1, 0.2, 0.3, 0.4 and 0.5

m). The wind approched the the turbine with a wind speed of U_{wu}. The wind speed decreases as it approaches the turbine before it passes thorugh the rotor plane. The axial velocity deficit is the amount of decrease in the frestream velocity. The induction factor *a* given by the equation 9 represnets the fraction by which the axial component of the velocity is reduced. The axial component of the velocity reduces further after passing the rotor plane (y = 0.1, 0.2, 0.3, 0.4 and 0.5 m) as shown in Fig. 4. There is a pressure drop across the rotor plane when the air passes the rotor plane. Downtream the rotor plane, the pressure is recovered and back to the atomospheric pressure where the average air velocity is U_{wd} as shown in Fig. 5. This average air velocity downtream the wind turbine and where the pressure is recovered back to the atmospheric pressure is used to calculate the induction factor using the equations 9 and 10. The Cp is then caluclated using the equation 8 for the unshrouded turbine. The variation of the Cp and *a* with the tip speed ratio are show in Fig. 6. The results show a maximum value for Cp of 0.38 at a tip speed ratio bewteen 7 and 8. The value of Cp dereases to 0.2 at low and high tip speed ratio (TSR = 4 and TSR = 10). The induction factor a for the range of TSR tested in the present study was between 0.06 and 0.13. The maxium value for the induction factor a = 0.13 was obatined at TSR = 7 and is less than the maximum theoretical value of inducton fcator of a = 1/3 (Betz limit).

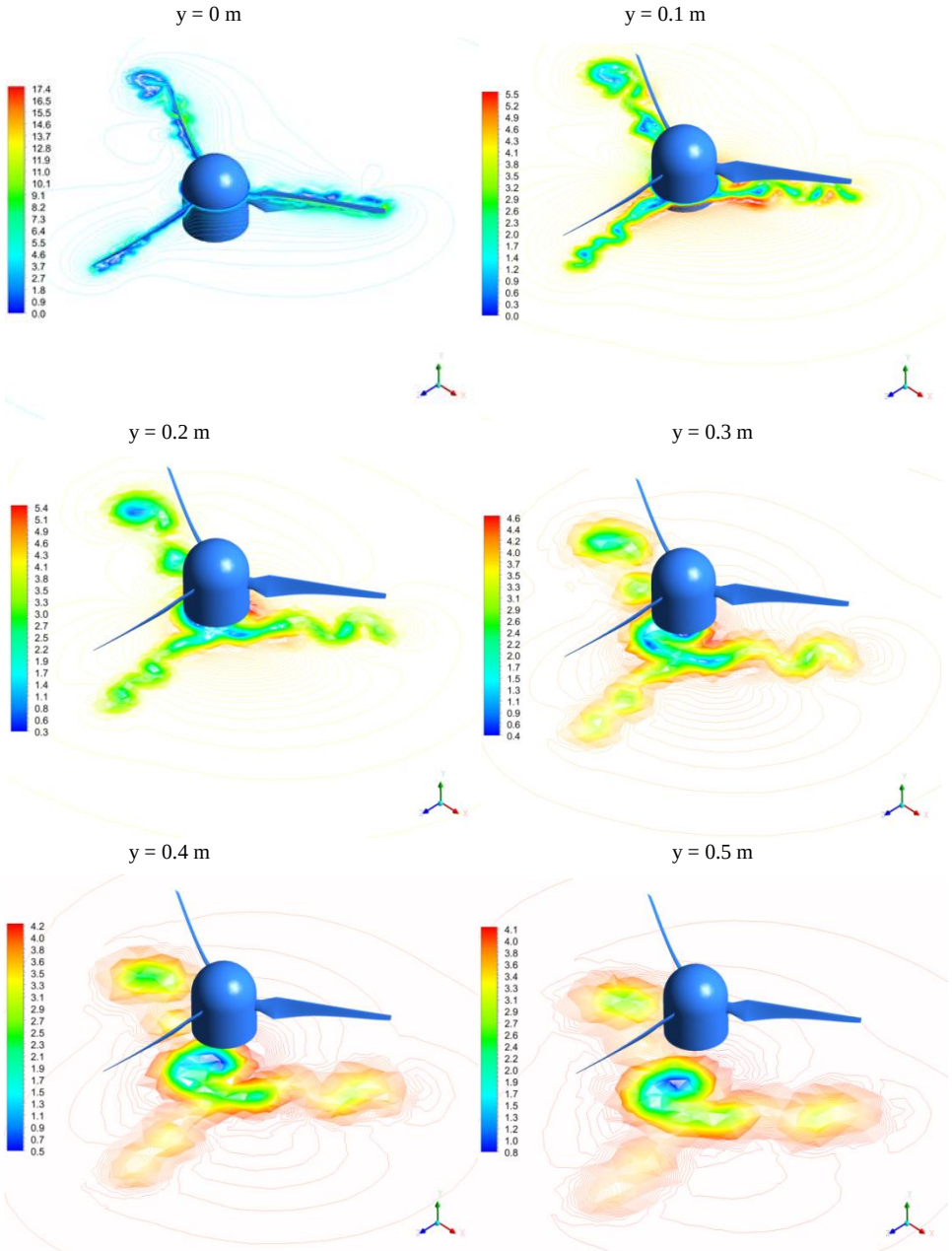

Figure 4: Velocity magnitude at the rotor plane and at different stations behind the wind turbine: Unshrouded Turbine, U_{wu} = 4 m/s and TSR = 7

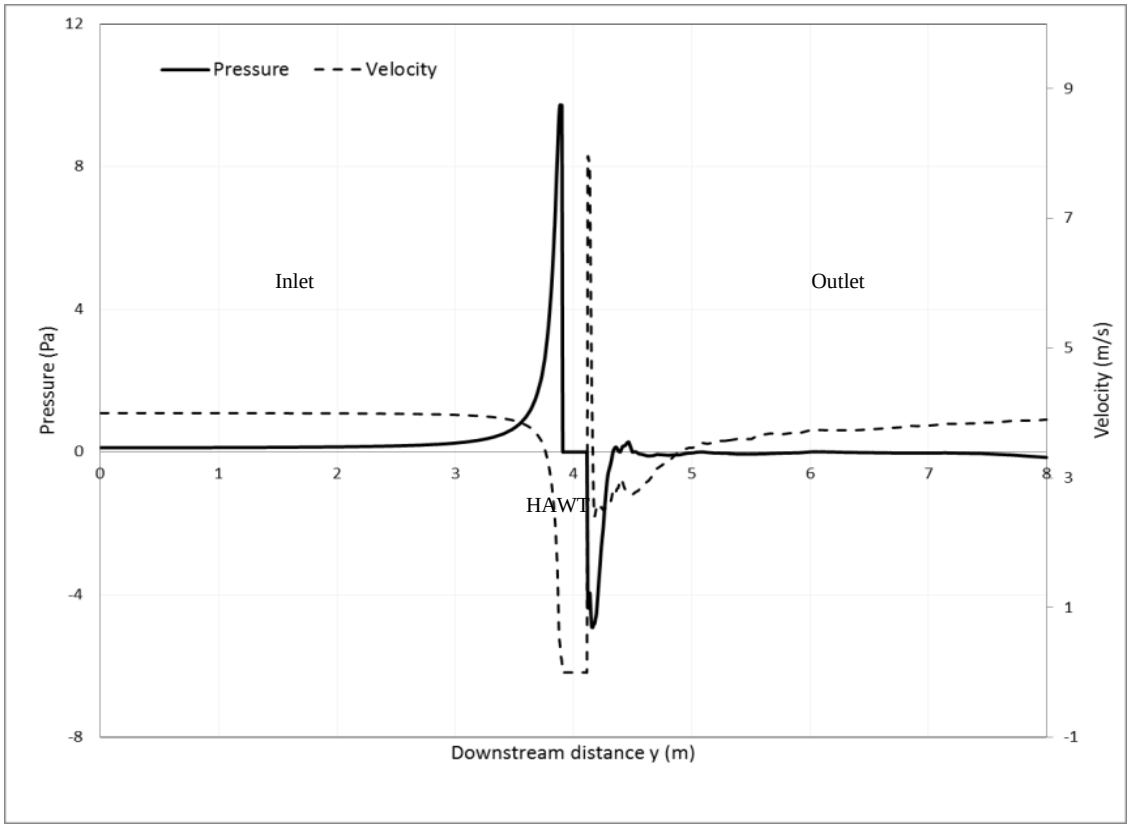

Figure 5: Axial variation of the pressure and velocity magnitde for the Unshouded Wind Turbine (U_{wu} = 4 m/s, and TSR = 7)

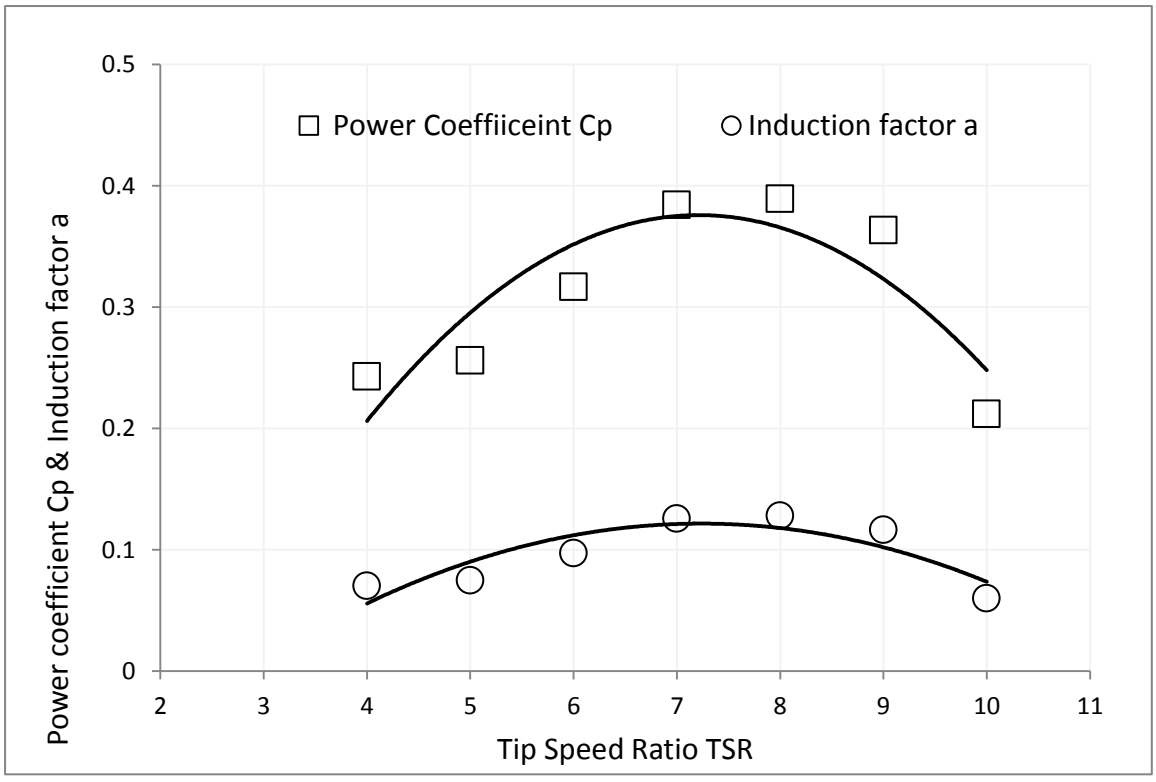

Figure 6: Power coefficient Cp and induction factor a for the unshrouded wind turbine

For the shrouded turbine, the equations 11-14 are used to calculate the C_p. The area ratio, $\varepsilon_{L,}$ was calculated using the selected geometry of the shroud (A_{out}/A_{rot}). The back pressure coefficient, μ, was calculated using equation 13 based on the average wind speed at the exit of the shroud U_{out}. Figs. 7 and 8 show the velocity magnitude in the X-Y and X-Z planes respectively; for the shrouded wind turbine. The velocity contour results show clearly an increase (1.8 times the freestream velocity U_{wu} = 4 m/s) of the wind speed inside the shrouded turbine. This will draw more mass flow inside the shrouded wind turbine leading to an increase in the shaft power, i.e., the power extracted from the turbine.

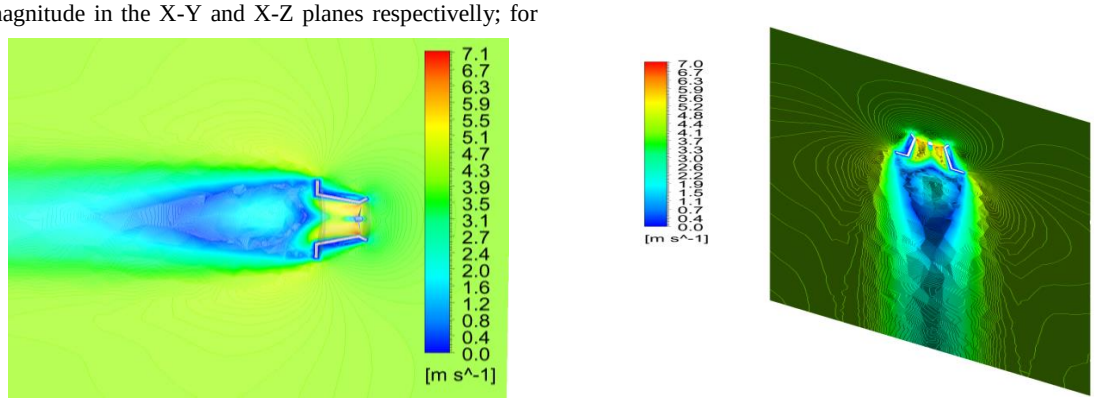

Figure 7: Velocity magnitude contours in the X-Y plane for the shrouded turbine (U_{wu} = 4 m/s and TSR = 7)

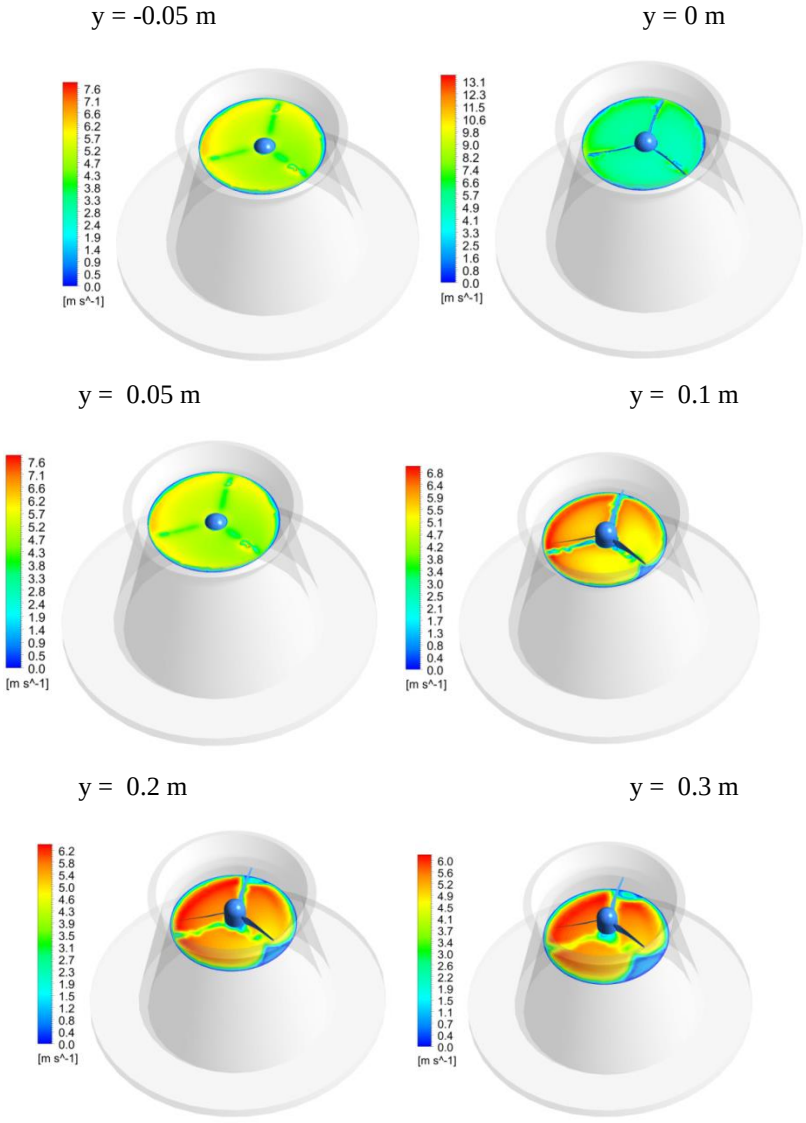

Figure 8: Velocity magnitude contours in the X-Z plane for the shrouded turbine (U_{wu} = 4 m/s and TSR = 7)

Like the unshrouded turbine, the wind approched the shrouded wind turbine with a wind speed of U_{wu} = 4 m/s. The wind speed decreases as it approaches the turbine before it passes thorugh the rotor plane. The axial velocity deficit is the amount of decrease in the frestream velocity, as shown in Fig. 9. The induction factor $\bar{a}$ given by the equation 16 represents the fraction by which the axial component of the velocity is reduced. The average air velocity downtream the wind turbine and where the pressure is recovered back (See Fig. 9) to the atmospheric pressure is used to calculate the induction factor. The back pressure coefficient is calculated from the average wind speed at the shroud exit using equation 13. The power coefficient Cp is then caluclated using the equation 11 for the shrouded turbine. The power coefficients versus the TSR were then determined for the shrouded turbines as shown in Figure 10. The results in Fig. 10 show an increase of the Cp by a factor ranging from 2.46 to 4.33 for the shrouded turbine compared to unshrouded turbine. The numerical results show a net improvement and more pronounced enhancement of the electrical power extracted from the shrouded turbine. These results are in good agreement with the experimental data obtained by Yuji and Takashi [6] for the shrouded wind turbine with a brimmed diffuser. His experimental results show a power augmentation by a factor of about 2–5 compared with a bare wind turbine, for a given turbine diameter and wind speed. The experimental results also show that for long diffuser (Diffuser length Lt = 1.47 D), a remarkable increase in the output power of approximately 4-5 times that of a conventional wind turbine is achieved [6].

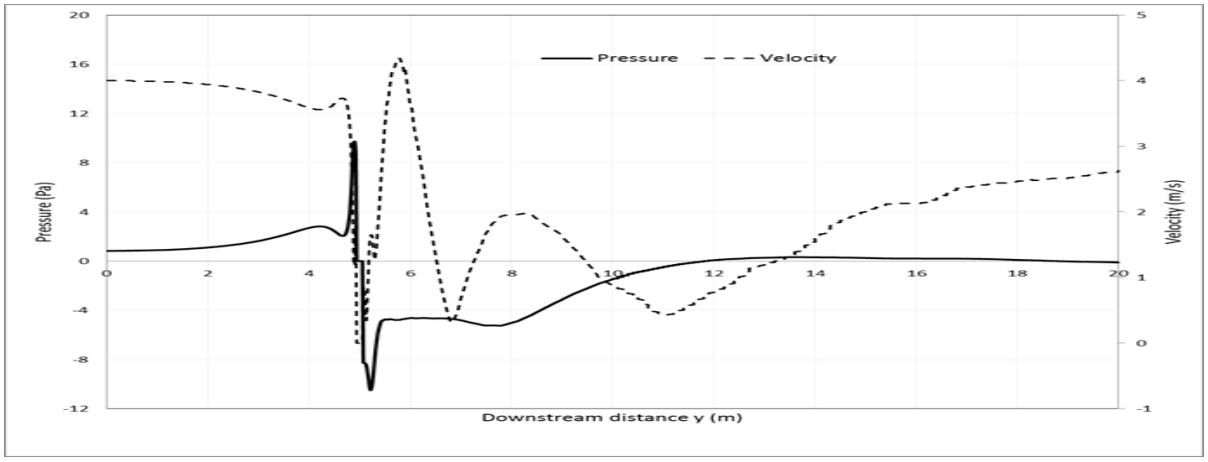

Figure 9: Axial variation of the pressure and velocity magnitde for the shouded Wind Turbine (U_{wu} – 4 m/s, and TSR = 7)

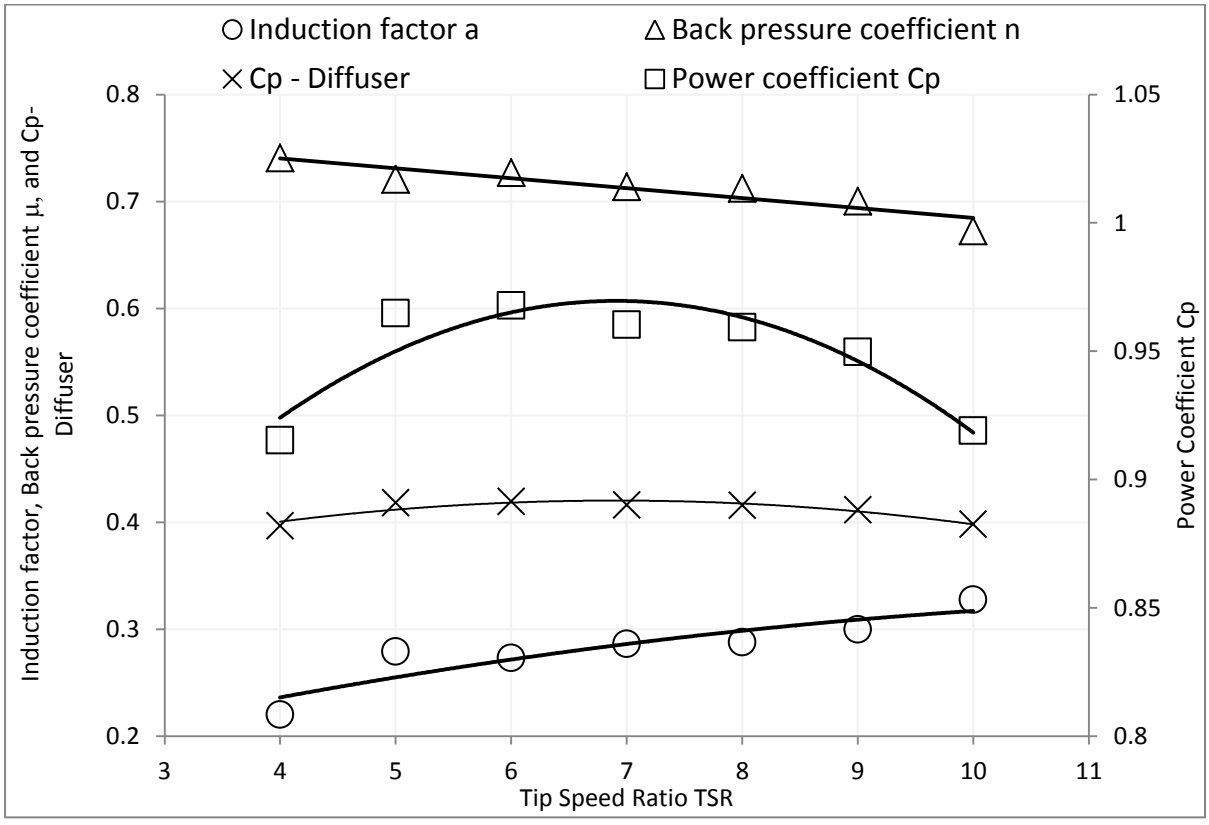

Figure 10: Variation of the power coefficient Cp and induction factor $\bar{a}$ with the tip speed ratio - Shrouded wind turbine (Uwu = 4 m/s)

6. Conclusions

Computational fluid dynamics analysis was performed in the present study to assess the performance of shrouded HAWT. The governing equations of mass, momentum and turbulence equations were solved using finite volume method to obtain the information about the flow field around the turbine. The induction factor and the power coefficient (Cp) were calculated from the computed velocity profiles. The Computational Fluid Dynamics results and the variation of the Cp versus the tip speed ratio of the unshrouded and shrouded turbines show that the shrouded turbines can generate greater power than the non-shrouded baseline wind turbine; and the variation of the Cp versus the tip speed ratio shows an increase by a four folds compared to the unshrouded turbine. This increase is due to the increase of the air speed inside the shrouded turbines. The present study suggests that shrouded HAWT can be a good solution for energy production in regions with low speed conditions offsetting more fossil fuel usage and reducing their subsequent greenhouse gas emissions.

References

[1] Chaouki Ghenai, Isam Janajreh, Comparison of resource intensities and operational parameters of renewable, fossil fuel, and nuclear power systems, International Journal of Thermal and Environmental Engineering, Volume 5, No2, 95-104, 2013.

[2] Kanyako F. , Isam Janajreh, Implementation and economical study of HAWT under different wind, Sustainable Cities and Society, 15, 2015, 153-160.

[3] Lew, D. (2000). Alternative to coal and candles: wind power in China. Energy Policy, 28, 271-286.

[4] Hjort S., and Larsen, H., Rotor design for diffuser augmented wind turbines, Energies, 8, 10736-10774, 2015.

[5] Maia, L.A.B, Experimental and Numerical study of diffuser augmented wind turbine, DAWT, Master thesis, December 2014.

[6] Yuji Ohya and Takahi Krasudani, A Shrouded wind turbine generating high output power with wind lens technology, Energies, 3, 634-649, 2010.

[7] Buyung Kosasih, and Andrea Tondelli, Experimental study of shrouded micro-wind turbine, Evolving Energy-IEFInternational Energy Congress (IEF-IEC2012), Procedia Engineering 49 (2012), 92 – 98.

[8] Jun-Feng Hu, and Wen-Xue Wang, Upgrading a Shrouded Wind Turbine with a Self-Adaptive Flanged Diffuser, Energies 8, 2015, 5319-5337.

[9] Aniket C. Aranake, Vinod K. Lakshminarayan, and Karthik Duraisamy, Computational analysis of shrouded wind turbine configurations using a 3-dimensional RANS solver, Renewable Energy 75 (2015) 818-832.

[10] Aly M. El-Zahaby, A.E. Kabeel, , S.S. Elsayed, M.F. Obiaa, CFD analysis of flow fields for shrouded wind turbine's diffuser model with different flange angles, Alexandria Engineering Journal, 56, Issue 1, 2017, 171–179.

[11] Isam Janajreh, Ilham Talab, Wind Data Collection and Analyses at Masdar City for Wind TurbineAssessment, Int. J. of Thermal & Environmental Engineering , Vol. 1, No. 1 (2010) 43-50.

[12] Isam Janajreh, Ilham Talab, and Jill Macpherson, Numerical Simulation of Tower Rotor Interaction for Downwind Wind Turbine, Hindawi: Modelling and Simulation in Engineering, Volume 2010, Article ID 860814, 11 pages, doi:10.1155/2010/860814.

[13] Ghenai, C., Sargsyan, A., and Janajreh, I., Three dimensional modeling of flow field around a horizontal axis wind turbine (HAWT), Computational Fluid Dynamics in the Development of Renewable Energy Applications Book, International Energy and Environment Foundation, 2011.

[14] I Janajreh, R Qudaih, I Talab, C Ghenai, Aerodynamic flow simulation of wind turbine: downwind versus upwind configuration, Energy Conversion and Management 51 (8), 1656-1663.

[15] Patankar, S. V. (1980). Numerical Heat Transfer and Fluid Flow. Taylor & Francis. ISBN 978-0-89116-522-4.

[16] Ferziger, J. H.; Peric, M. (2001). Computational Methods for Fluid Dynamics. Springer-Verlag. ISBN 978-3-540-42074-3.

[17] Tannehill, J. C.; Anderson, D. A.; Pletcher, R. H. (1997). Computational Fluid Mechanics and Heat Transfer. Taylor & Francis.

[18] Bussel, G.J.W., An assessment of the performance of diffuser augmented wind turbines, Delft University of Technology, Proceedings of the 3th ASME Joint Fluids Engineering Conference, San Francisco, California, July 18-23, 1999.

[19] Bussel, G.J.W., The Science of making more torque from wind: diffuser experiment and theory revisited, Delft University of Technology, Journal of Physics confer.